
Kronecker-factored Quasi-Newton Methods for Deep Learning

Yi Ren¹ Achraf Bahamou¹ Donald Goldfarb¹

Abstract

Second-order methods have the capability of accelerating optimization by using much richer curvature information than first-order methods. However, most are impractical for deep learning, where the number of training parameters is huge. In Goldfarb et al. (2020), practical quasi-Newton methods were proposed that approximate the Hessian of a multilayer perceptron (MLP) model by a layer-wise block diagonal matrix where each layer’s block is further approximated by a Kronecker product corresponding to the structure of the Hessian restricted to that layer. Here, we extend these methods to enable them to be applied to convolutional neural networks (CNNs), by analyzing the Kronecker-factored structure of the Hessian matrix of convolutional layers. Several improvements to the methods in Goldfarb et al. (2020) are also proposed that can be applied to both MLPs and CNNs. These new methods have memory requirements comparable to first-order methods and much less per-iteration time complexity than those in Goldfarb et al. (2020). Moreover, convergence results are proved for a variant under relatively mild conditions. Finally, we compared the performance of our new methods against several state-of-the-art (SOTA) methods on MLP autoencoder and CNN problems, and found that they outperformed the first-order SOTA methods and performed comparably to the second-order SOTA methods.

1. Introduction

First-order methods, including stochastic gradient descent (SGD) (Robbins & Monro, 1951) and the class of adaptive learning rate methods, such as AdaGrad (Duchi et al., 2011), RMSprop (Hinton et al., 2012), and Adam (Kingma & Ba, 2014), are currently the most popular methods for training deep neural networks (DNNs), including multilayer perceptrons (MLPs) and convolutional neural networks (CNNs), etc. Although these methods are fairly easy to implement, they use, at most, a very limited amount of curvature information to facilitate optimization. Vanilla SGD uses no curvature information, while the adaptive learning rate methods use a diagonal pre-conditioning matrix based on the second moment of the gradient.

On the other hand, second-order methods use the rich curvature information of the problem to accelerate optimization. Beside the classical Newton method, sub-sampled Newton methods have been proposed to handle large data sets (see e.g., Xu et al. (2019)), but when the number of training parameters is huge, inverting the Hessian matrix is impractical. Hence, quasi-Newton (QN) methods, ranging from the original BFGS (Broyden, 1970; Fletcher, 1970; Goldfarb, 1970; Shanno, 1970) and limited-memory BFGS (L-BFGS) (Liu & Nocedal, 1989), to more recent developments that take into account stochasticity and/or non-convexity (Byrd et al., 2016; Gower et al., 2016; Wang et al., 2017), have been considered. Other methods use surrogates to the Hessian, such as the Gauss-Newton (GN) and Fisher matrices (e.g., natural gradient (NG) method (Amari et al., 2000), Hessian-free method (Martens, 2010), Krylov subspace method (Vinyals & Povey, 2012), sub-sampled GN and NG methods (Ren & Goldfarb, 2019), etc). However, in all of the above-mentioned second-order methods, whether they use the Hessian or a surrogate, the size of the curvature matrix becomes prohibitive when the number of training parameters is huge.

Consequently, second-order methods for training DNNs have been proposed that make use of layer-wise block-diagonal approximations to Hessian and Fisher matrices, where each diagonal block is further approximated as the Kronecker product of smaller matrices to reduce their memory and computational requirements. One of the most popular methods of this type is the NG method KFAC, which was originally proposed for MLPs (Martens & Grosse, 2015), and later extended to CNNs

¹Department of Industrial Engineering and Operations Research, Columbia University, New York NY, USA. Correspondence to: Yi Ren <yr2322@columbia.edu>.

(Grosse & Martens, 2016) and other models (Wu et al., 2017; Martens et al., 2018). Other Kronecker-factored NG methods have also been proposed in Heskes (2000); Povey et al. (2014); George et al. (2018). A Kronecker-factored QN method (which we will refer to as K-BFGS-20) was proposed in Goldfarb et al. (2020). This method was only designed for MLPs and serves as the starting point for the methods developed in this paper. The approximate generalized GN method KFRA (Botev et al., 2017) adopts a block-diagonal Kronecker-factored approximation to the GN matrix for MLPs and computes the diagonal block approximations recursively. Finally, Shampoo (Gupta et al., 2018) and TNT (Ren & Goldfarb, 2021) also use block-diagonal Kronecker-factored pre-conditioning matrices, stemming from adaptive learning rate methods and natural gradient methods, respectively

1.1. Our Contributions

In this paper, we propose brand new versions of K-BFGS, that are substantial extensions to the Kronecker-factored quasi-Newton methods for MLPs proposed in Goldfarb et al. (2020). Not only can they be applied to CNNs, but they also incorporate several generic improvements beyond what was proposed in Goldfarb et al. (2020).

In order to enable K-BFGS to train CNN models, we first show that for a convolutional layer, the gradient and Hessian restricted to that layer can be approximated by the Kronecker product of two vectors and matrices, respectively, extending the results in Botev et al. (2017); Wu et al. (2020), etc. We then formalize exactly how K-BFGS should be applied to optimize the parameters in convolutional layers, with the Kronecker-factored approximation of the Hessian as the basis.

Our generic improvements to Goldfarb et al. (2020) include a new double damping technique $D_P D_{LM}$ and a "minibatched" Hessian-action BFGS, both of which are applicable to convolutional and fully-connected layers.

Our proposed methods have comparable memory requirements to those of first-order methods, while their per-iteration time complexities are smaller, and in many cases, much smaller than those of Goldfarb et al. (2020) and other popular second-order methods such as KFAC. Further, we prove convergence results for a limited memory K-BFGS(L) variant under relatively mild conditions.

We conducted experiments on several MLP autoencoder problems, which demonstrated that our improved versions of K-BFGS outperformed the ones proposed in Goldfarb et al. (2020). Moreover, on several well-studied CNN problems, our proposed method outperformed the 1st-order SOTA methods SGD-m (i.e., SGD with momentum) and Adam and performed comparably to the 2nd-order SOTA method KFAC.

2. Kronecker-factored Structures in CNNs

In this section, after first discussing the computations involved in a CNN model, we describe the Kronecker structures of the gradient and Hessian of the loss function with respect to a convolutional layer's parameters.

2.1. Convolutional Neural Networks (CNNs)

We consider a CNN with L trainable layers (for simplicity, assume they are all convolutional layers), with parameters consisting of a weight tensor w_l and a bias vector b_l (shapes specified later) for $l \in \{1, \dots, L\}$ and a loss function \mathcal{L} . For a data-point (x, y) , x is fed into the CNN as input, yielding \hat{y} as the output. The loss $\mathcal{L}(\hat{y}, y)$ between the output \hat{y} and y is a non-convex function of the set of all trainable parameters $\theta := \{w_1, b_1, \dots, w_L, b_L\}$.

For a dataset that contains multiple data-points indexed by $n = 1, \dots, N$, let $f(n; \theta)$ denote the loss from the n th data-point. Thus, viewing the dataset as an empirical distribution, the actual loss function that we wish to minimize is

$$f(\theta) := \mathbb{E}_n[f(n; \theta)] := \frac{1}{N} \sum_{n=1}^N f(n; \theta).$$

Let us now focus on a single convolutional layer of the CNN, with its own weight tensor w and bias vector b as the trainable parameters. For simplicity, we omit the layer index l , and assume that:

1. the convolutional layer is 2-dimensional;
2. the filters are of size $(2R + 1) \times (2R + 1)$, with spatial offsets from the centers of each filter indexed by $\delta \in \Delta := \{-R, \dots, R\} \times \{-R, \dots, R\}$;

3. the stride is of length 1, and the padding is equal to R , so that the sets of input and output spatial locations ($t \in \mathcal{T} \subset \mathbb{R}^2$) are the same.¹;
4. the layer has J input channels indexed by $j = 1, \dots, J$, and I output channels indexed by $i = 1, \dots, I$.

The weight tensor $w \in \mathbb{R}^{I \times J \times (2R+1) \times (2R+1)}$ corresponds to the elements of all of the filters in the layer. Hence, an element of w is denoted as $w_{i,j,\delta}$, where the first two indices i, j are the output/input channels, and the last two indices δ are the spatial offset within a filter. The bias $b \in \mathbb{R}^I$ is a length- I vector.

Let a , with components $a_{j,t}$, denote the input to the layer after padding is added, where t denotes the spatial location of the padded input and $j = 1, \dots, J$; and let h , with components $h_{i,t}$, denote the output of the layer, where t denote the spatial location of the output and $i = 1, \dots, I$. Given a , h is computed as

$$h_{i,t} = \sum_{j=1}^J \sum_{\delta \in \Delta} w_{i,j,\delta} a_{j,t+\delta} + b_i, \quad t \in \mathcal{T}, i = 1, \dots, I. \quad (1)$$

Note that we only consider the linear transformation of the convolutional layer. In other words, if there is any activation or any other operations such as batch normalization afterwards, we view it as being separate from the layer.

2.2. Kronecker-factored Structure of Gradient and Hessian for Convolutional Layers

Recent work has shown that curvature information in DNNs has the property of being a sum (or average, equivalently) of Kronecker products, beginning with the development of KFAC (Martens & Grosse, 2015; Grosse & Martens, 2016), which showed this for Fisher matrices. Botev et al. (2017) and Goldfarb et al. (2020) showed that Hessian matrices are also a sum of Kronecker product for fully-connected layers, while Bakker et al. (2018) and Wu et al. (2020) extended this result to convolutional layers.

Based on the above Kronecker-factored structures, practical second-order methods for deep learning models were proposed, by approximating the curvature as a single Kronecker product, including KFAC (Martens & Grosse, 2015; Grosse & Martens, 2016), KFRA (Botev et al., 2017), and K-BFGS-20 (Goldfarb et al., 2020).

Without developing any training method, Wu et al. (2020) proposed a single Kronecker product approximation to the Hessian of a DNN that consists of alternating convolutional layers and ReLU activation functions, without any further modifications, such as batch normalization or skip connections. Moreover, assuming all activation functions are ReLU results in the "second order" term in the Hessian being zero and the Hessian being equivalent to a Gauss-Newton matrix (or equivalently, a Fisher matrix). In contrast, we show that the Hessian has a Kronecker-factor structure for convolutional layers, without any assumptions about the activation functions or model architectures.

2.2.1. CASE 1: SINGLE DATA-POINT

We now consider a single data-point, omitting the index n for simplicity, and derive the structure of gradient and Hessian with respect to the loss function $f(\cdot; \theta)$.

We define $\mathcal{D}X := \frac{\partial f}{\partial X}$ for any variable X and $\text{vec}(\cdot)$ to be the vectorization of a matrix. For the output and input of the layer, we define, respectively, the vectors

$$\mathbf{h}_t := (h_{1,t}, \dots, h_{I,t})^\top \in \mathbb{R}^I,$$

$$\mathbf{a}_t := (a_{1,t+\delta_1}, \dots, a_{J,t+\delta_{|\Delta|}}, 1)^\top \in \mathbb{R}^{J|\Delta|+1},$$

for $t \in \mathcal{T}$. Note that a homogeneous coordinate is concatenated at the end of \mathbf{a}_t .

For the weights and biases, we define the vectors

$$\mathbf{w}_i := (w_{i,1,\delta_1}, \dots, w_{i,J,\delta_{|\Delta|}}, b_i)^\top \in \mathbb{R}^{J|\Delta|+1},$$

for $i = 1, \dots, I$, and from them the matrix

$$W := (\mathbf{w}_1, \dots, \mathbf{w}_I)^\top \in \mathbb{R}^{I \times (J|\Delta|+1)}, \quad (2)$$

¹The derivations in this paper can also be extended to the case where stride is greater than 1.

which contains all the parameters of the convolutional layer.

The following Theorem 2.1 gives the structure of gradient and Hessian of W for a single data-point, the proof of which can be found in Section B in the Appendix.

Theorem 2.1. *For a single data-point,*

i) (Structure of gradient)

$$\text{vec}(DW) = \sum_{t \in \mathcal{T}} \mathbf{a}_t \otimes D\mathbf{h}_t$$

is the sum of $|\mathcal{T}|$ Kronecker products;

ii) (Structure of Hessian)

$$\frac{\partial^2 f}{\partial \text{vec}(W)^2} = \sum_{t, t' \in \mathcal{T}} A_{t, t'} \otimes G_{t, t'}$$

is the sum of $|\mathcal{T}|^2$ Kronecker products, where

$$\begin{aligned} A_{t, t'} &:= \mathbf{a}_t \mathbf{a}_{t'}^\top \in \mathbb{R}^{(J|\Delta|+1) \times (J|\Delta|+1)}, \\ G_{t, t'} &:= \frac{\partial^2 f}{\partial \mathbf{h}_t \partial \mathbf{h}_{t'}} \in \mathbb{R}^{I \times I}. \end{aligned} \quad (3)$$

for $t, t' \in \mathcal{T}$.

If we **assume** that $G_{t, t'} = 0$ for $t \neq t'$, we have that

$$\frac{\partial^2 f}{\partial \text{vec}(W)^2} \approx \sum_{t \in \mathcal{T}} A_{t, t} \otimes G_{t, t}. \quad (4)$$

As in other methods that have been proposed for training DNNs that use Kronecker factored approximations to Hessian or other pre-conditioning matrices (Martens & Grosse, 2015; Grosse & Martens, 2016; Botev et al., 2017; Goldfarb et al., 2020), we further approximate $\frac{\partial^2 f}{\partial \text{vec}(W)^2}$ by a single Kronecker product. To achieve this, we now approximate the average of the Kronecker products of a set of matrix pairs $\{(U_t, V_t)\}$ by the Kronecker product of the averages of individual sets of matrices $\{U_t\}, \{V_t\}$, i.e.,

$$\frac{1}{|\mathcal{T}|} \sum_{t \in \mathcal{T}} U_t \otimes V_t \approx \left(\frac{1}{|\mathcal{T}|} \sum_{t \in \mathcal{T}} U_t \right) \otimes \left(\frac{1}{|\mathcal{T}|} \sum_{t \in \mathcal{T}} V_t \right). \quad (5)$$

Applying (5) to (4), we have that

$$\begin{aligned} \frac{\partial^2 f}{\partial \text{vec}(W)^2} &\approx |\mathcal{T}| \cdot \left(\frac{1}{|\mathcal{T}|} \sum_{t \in \mathcal{T}} A_{t, t} \right) \otimes \left(\frac{1}{|\mathcal{T}|} \sum_{t \in \mathcal{T}} G_{t, t} \right) \\ &= \left(\sum_{t \in \mathcal{T}} A_{t, t} \right) \otimes \left(\frac{1}{|\mathcal{T}|} \sum_{t \in \mathcal{T}} G_{t, t} \right). \end{aligned} \quad (6)$$

Note that the assumptions we made in deriving (6) are analogous to the IAD (Independent Activations and Derivatives), SH (Spatial Homogeneity), and SUD (Spatially Uncorrelated Derivatives) assumptions in Grosse & Martens (2016). Lastly, one can similarly derive a single Kronecker approximation for the gradient, using Theorem 2.1 and (5).

2.2.2. CASE 2: MULTIPLE DATA-POINTS

In the case of multiple data-points, we use (n) to denote the index of a data-point. To approximate the average Hessian across multiple data-points as a single Kronecker product, we again use (5), but averaging over the data points this time. By

(6), we have that

$$\begin{aligned} \frac{\partial^2 f}{\partial \text{vec}(W)^2} &= \mathbb{E}_n \left[\frac{\partial^2 f(n)}{\partial \text{vec}(W)^2} \right] \\ &\approx \mathbb{E}_n \left[\left(\sum_{t \in \mathcal{T}} A_{t,t}(n) \right) \otimes \left(\frac{1}{|\mathcal{T}|} \sum_{t \in \mathcal{T}} G_{t,t}(n) \right) \right] \end{aligned} \quad (7)$$

$$\approx A \otimes G, \quad (8)$$

where

$$A := \mathbb{E}_n \left[\sum_{t \in \mathcal{T}} A_{t,t}(n) \right], G := \mathbb{E}_n \left[\frac{1}{|\mathcal{T}|} \sum_{t \in \mathcal{T}} G_{t,t}(n) \right]. \quad (9)$$

(8) will serve as the foundation for us to develop the Kronecker-factored QN method for CNNs below.

3. Our New K-BFGS Method

3.1. K-BFGS-20 in Goldfarb et al. (2020)

For the Kronecker-factored quasi-Newton method that Goldfarb et al. (2020) proposed for training multilayer perceptrons (MLPs), they approximated the Hessian of the loss function by a block diagonal matrix, where each block corresponds to the Hessian w.r.t. the parameters of a fully-connected layer. As a result, the parameters of each layer can be updated separately.

For a single fully-connected layer in the MLP, Goldfarb et al. (2020) approximates the Hessian restricted to that layer as $H_A \otimes H_G$, where H_A and H_G are some approximations to some matrices A^{-1} and G^{-1} , respectively. As a result, by the property of Kronecker product, they update the parameters of this fully-connected layer by computing

$$W^+ = W - \alpha H_G (\mathcal{D}W) H_A, \quad (10)$$

where W denotes the parameters (including weights and biases) in the fully-connected layer and α denotes the learning rate.

Furthermore, in Goldfarb et al. (2020), H_A and H_G , as the approximations to A^{-1} and G^{-1} , are estimated with the BFGS (or L-BFGS) updating formula. To be more specific, given an approximation H_G to the inverse of a symmetric matrix G , the BFGS updating formula computes

$$H_G^+ = (I - \rho \mathbf{s}_G \mathbf{y}_G^\top) H (I - \rho \mathbf{y}_G \mathbf{s}_G^\top) + \rho \mathbf{s}_G \mathbf{s}_G^\top, \quad (11)$$

with given vectors $\mathbf{s}_G, \mathbf{y}_G$ and $\rho = \frac{1}{\mathbf{y}_G^\top \mathbf{s}_G}$. H_A is similarly computed with BFGS updating.

Lastly, the $(\mathbf{s}_G, \mathbf{g}_G)$ pairs used by H_G is derived from the definition of G as a Hessian matrix w.r.t. the output of the fully-connected layer. A double damping procedure with damping term λ_G is proposed to deal with the non-convexity of G . For H_A , Goldfarb et al. (2020) keeps track of an estimation to A and generate the $(\mathbf{s}_A, \mathbf{y}_A)$ pairs with a "Hessian-action" approach, i.e. letting $\mathbf{s}_A = A \mathbf{y}_A + \lambda_A \mathbf{s}_A$, where λ_A is the damping term.

3.2. What's New in Our K-BFGS Method?

In this part, we describe the generic improvements of our new methods beyond K-BFGS-20, as well as how to extend the methods to convolutional layers. The complete pseudo-code and other implementation details are described in Sec A in the Appendix.

3.2.1. GENERIC IMPROVEMENTS BEYOND K-BFGS-20

Improvement #1: $D_P D_{LM}$. In the double damping procedure proposed in Goldfarb et al. (2020), the parameter μ_2 can only take values in $(0, 1]$, which restricts its interpretation as a Levenberg-Marquardt (LM) damping term.

We propose a new procedure $D_P D_{LM}$ (Algorithm 1), in which the parameter $\mu_2 (= \lambda_G)$ is more directly related to LM damping and can take any values in $(0, \infty)$. To see this connection, note that in Algorithm 1, after Powell's damping on H ,

Algorithm 1 $D_P D_{LM}$ (P stands for Powell’s damping and LM stands for Levenberg-Marquardt damping)

```

1: Input:  $\mathbf{s}, \mathbf{y}$ ; Output:  $\tilde{\mathbf{s}}, \tilde{\mathbf{y}}$ ; Given:  $H, 0 < \mu_1 < 1, \mu_2 > 0$ 
2: if  $\mathbf{s}^\top \mathbf{y} < \mu_1 \mathbf{y}^\top H \mathbf{y}$  then
3:    $\theta_1 = \frac{(1-\mu_1)\mathbf{y}^\top H \mathbf{y}}{\mathbf{y}^\top H \mathbf{y} - \mathbf{s}^\top \mathbf{y}}$ 
4: else
5:    $\theta_1 = 1$ 
6: end if
7:  $\tilde{\mathbf{s}} = \theta_1 \mathbf{s} + (1 - \theta_1) H \mathbf{y}$  {Powell’s damping on  $H$ }
8:  $\tilde{\mathbf{y}} = \mathbf{y} + \mu_2 \tilde{\mathbf{s}}$  {Levenberg-Marquardt damping on  $H^{-1}$ }
9: return:  $\tilde{\mathbf{s}}, \tilde{\mathbf{y}}$ 
    
```

$\tilde{\mathbf{s}}^\top \mathbf{y} \geq \mu_1 \mathbf{y}^\top H \mathbf{y} \geq 0$. Hence, $\tilde{\mathbf{s}}^\top \tilde{\mathbf{y}} \geq \mu_2 \|\tilde{\mathbf{s}}\|^2$, which can be viewed as LM damping with a parameter of μ_2 , since G is then lower bounded by $\mu_2 I$.

Improvement #2: ”minibatched” Hessian-action BFGS. In approximating A^{-1} , Goldfarb et al. (2020) uses the so-called ”Hessian-action” approach, in which they compute As_A with an estimation of A from a moving average scheme with a given hyper-parameter on decaying. In other words, one needs to compute A from each minibatch and always keep track of a moving average of it, which could be time consuming when A is large. The large size of A is particularly true for convolutional layers.

In this paper, we propose a ”minibatched” version of Hessian-action BFGS, i.e. computing As with A estimated from only the current minibatch. By doing so, we avoid the explicit computation of A , replacing it with a direct matrix-vector product As . Moreover, the hyper-parameter on decaying is no longer needed, which could potentially save effort in hyper-parameter tuning. This improvement is applicable to both fully-connected and convolutional layers, the latter of which is described in Section 3.2.2.

3.2.2. EXTENSION TO CONVOLUTIONAL LAYERS

For convolutional layers, we similarly use (10) to update the parameters W defined in (2), where H_G and H_A corresponds to some approximations to the inverse of G and A defined in (9).

To approximate the inverse of G defined in (9), i.e. computing H_G , we use the BFGS updating formula (11), or L-BFGS. (We name our method K-BFGS and K-BFGS(L), respectively, when BFGS or L-BFGS is used for estimating H_G .) For a fixed data-point index n and $t \in \mathcal{T}$, the (\mathbf{s}, \mathbf{y}) pair for $G_{t,t}(n) = \frac{\partial^2 f(n)}{\partial \mathbf{h}_t(n)^2}$ is $(\mathbf{s}, \mathbf{y}) = (\mathbf{h}_t^+(n) - \mathbf{h}_t(n), \mathcal{D}\mathbf{h}_t^+(n) - \mathcal{D}\mathbf{h}_t(n))$, where the ”+” sign denotes that we compute the value after a step of the parameters has been taken. Hence, for a fixed n , the (\mathbf{s}, \mathbf{y}) pair for $\frac{1}{|\mathcal{T}|} \sum_{t \in \mathcal{T}} G_{t,t}(n)$ is $(\overline{\mathbf{h}^+}(n) - \overline{\mathbf{h}}(n), \overline{\mathcal{D}\mathbf{h}^+}(n) - \overline{\mathcal{D}\mathbf{h}}(n))$, where \overline{X} denotes the value of X_t averaged over the spatial locations \mathcal{T} for any quantity X , i.e., $\overline{X} := \frac{1}{|\mathcal{T}|} \sum_{t \in \mathcal{T}} X_t$. Finally, the (\mathbf{s}, \mathbf{y}) for G in (9) is

$$\mathbf{s}_G = \mathbb{E}_n \left[\overline{\mathbf{h}^+}(n) - \overline{\mathbf{h}}(n) \right], \quad (12)$$

$$\mathbf{y}_G = \mathbb{E}_n \left[\overline{\mathcal{D}\mathbf{h}^+}(n) - \overline{\mathcal{D}\mathbf{h}}(n) \right]. \quad (13)$$

Combining the above with the $D_P D_{LM}$ approach described in Section 3.2.1, the final (\mathbf{s}, \mathbf{y}) pair we use is $D_P D_{LM}(\mathbf{s}_G, \mathbf{y}_G)$.

To approximate the inverse of A defined in (9), i.e., computing H_A , we use the ”minibatched” Hessian-action BFGS described in Section 3.2.1. Given the current estimate H_A of A^{-1} , the (\mathbf{s}, \mathbf{y}) pair for updating H_A are computed as:

$$\mathbf{s}_A = H_A \hat{\mathbf{a}}, \quad \mathbf{y}_A = A \mathbf{s}_A + \lambda_A \mathbf{s}_A, \quad (14)$$

where $\hat{\mathbf{a}} = \mathbb{E}_n \left[\frac{1}{|\mathcal{T}|} \sum_{t \in \mathcal{T}} \mathbf{a}_t(n) \right] = \mathbb{E}_n \left[\overline{\mathbf{a}}(n) \right]$ and λ_A is the damping term. Since A is estimated from a minibatch, we

Table 1. Storage Requirement

Algorithm	DW	$DW \odot DW$	A / H_A	G / H_G	Total
K-BFGS	$O(IJ \Delta)$	—	$O(J^2 \Delta ^2)$	$O(I^2)$	$O(J^2 \Delta ^2 + IJ \Delta + I^2)$
K-BFGS(L)	$O(IJ \Delta)$	—	$O(J^2 \Delta ^2)$	$O(pI)$	$O(J^2 \Delta ^2 + IJ \Delta + pI)$
KFAC	$O(IJ \Delta)$	—	$O(J^2 \Delta ^2)$	$O(I^2)$	$O(J^2 \Delta ^2 + IJ \Delta + I^2)$
Adam	$O(IJ \Delta)$	$O(IJ \Delta)$	—	—	$O(IJ \Delta)$

Table 2. Computation per iteration beyond that required for the minibatch stochastic gradient

Algorithm	Additional pass	Curvature	Step ΔW_l
K-BFGS	$O\left(\frac{mIJ \Delta \mathcal{T} }{T}\right)$	$O\left(\frac{mJ \Delta \mathcal{T} + J^2 \Delta ^2 + mI \mathcal{T} + I^2}{T}\right)$	$O(IJ^2 \Delta ^2 + I^2J \Delta)$
K-BFGS(L)	$O\left(\frac{mIJ \Delta \mathcal{T} }{T}\right)$	$O\left(\frac{mJ \Delta \mathcal{T} + J^2 \Delta ^2 + mI \mathcal{T} + pI}{T}\right)$	$O(IJ^2 \Delta ^2 + pIJ \Delta)$
KFAC	$O\left(\frac{mIJ \Delta \mathcal{T} }{T_1}\right)$	$O\left(\frac{m(J^2 \Delta ^2 + I^2) \mathcal{T} }{T_1} + \frac{J^3 \Delta ^3 + I^3}{T_2}\right)$	$O(IJ^2 \Delta ^2 + I^2J \Delta)$
Adam	—	$O(IJ \Delta)$	$O(IJ \Delta)$

compute As_A without explicitly computing A . To be specific, by (3) and (9),

$$\begin{aligned}
 As_A &= \mathbb{E}_n \left[\sum_{t \in \mathcal{T}} \mathbf{a}_t(n) \mathbf{a}_t(n)^\top \right] s_A \\
 &= \mathbb{E}_n \left[\sum_{t \in \mathcal{T}} (\mathbf{a}_t(n)^\top s_A) \mathbf{a}_t(n) \right].
 \end{aligned} \tag{15}$$

Lastly, we propose to set the damping terms $\lambda_A = \sqrt{|\mathcal{T}|} \sqrt{\lambda}$, $\lambda_G = \frac{1}{\sqrt{|\mathcal{T}|}} \sqrt{\lambda}$ for a given overall damping hyper-parameter λ , which is shown to be better than setting $\lambda_A = \lambda_G = \sqrt{\lambda}$, which was proposed in Goldfarb et al. (2020) for fully-connected layers. (See Section A.3 in the Appendix for more discussion on this.)

4. Space and Computational Requirements

In this section, we compare the space and computational requirements of the proposed K-BFGS and K-BFGS(L) methods with KFAC (see Algorithm 5 in the Appendix) and Adam, which are among the predominant 2nd- and 1st-order methods, respectively, used to train CNNs. (One can also easily make similar comparison for MLPs.)

We focus on one convolutional layer, with J input channels, I output channels, kernel size $|\Delta|$, and $|\mathcal{T}|$ spacial locations. Moreover, let m denote the size of minibatches, p denote the number of (s, y) pairs for L-BFGS, T denote the curvature update frequency for K-BFGS/K-BFGS(L), and T_1 and T_2 denote the frequency of statistics update and inverse update for KFAC, respectively.

From Table 1, one can see that K-BFGS/K-BFGS(L) requires roughly the same amount of memory as KFAC. Note that I and J are usually much larger than $|\Delta|$ in CNNs. For example, in VGG16 (Simonyan & Zisserman, 2014), I and J can be as large as 512 whereas $|\Delta| = 9$. Hence, as Table 1 shows, the memory required by K-BFGS/K-BFGS(L) is of the same order as that of Adam in terms of I and J .

In Table 2, besides the operations listed, each algorithm also needs to compute the minibatch gradient requiring $O(mIJ|\Delta||\mathcal{T}|)$ time. (Note that $|\mathcal{T}|$ is usually much larger than I or J .) Comparing with K-BFGS-20, K-BFGS improves time complexity due to the usage of "minibatched" Hessian-action BFGS. If K-BFGS-20 were used (with original Hessian-action BFGS), the first term $O\left(\frac{mJ|\Delta||\mathcal{T}|}{T}\right)$ of the "Curvature" column for K-BFGS and K-BFGS(L) would increase to $O\left(\frac{mJ^2|\Delta|^2|\mathcal{T}|}{T}\right)$. K-BFGS requires considerably less time to compute curvature information than KFAC. First, K-BFGS avoids matrix inversion, whose complexity is $O(I^3)$ and $O(J^3|\Delta|^3)$ (although this is amortized in KFAC by $\frac{1}{T_2}$ by using

the same inverse for T_2 iterations). Second, K-BFGS avoids computing the Ω and Γ matrices of KFAC from minibatch data, whose complexity is $m(J^2|\Delta|^2 + I^2)|\mathcal{T}|$. Instead, we directly compute the (\mathbf{s}, \mathbf{y}) pairs for H_A and H_G , without explicitly forming A or G .

5. Convergence Results

In this section, we present convergence results for a variant of K-BFGS(L) (specifically, Algorithm 3 in the Appendix), following the framework in Wang et al. (2017). For the purpose of simplicity, we assume that all layers are convolutional. (Our results also hold for MLPs or if the model contains both convolutional and fully-connected layers.)

There are several minor difference (described in Section C in the Appendix) between Algorithm 3 and our actual implementation of K-BFGS(L). In particular, $D_{P(I)}D_{LM}$ (see Algorithm 4 in the Appendix), rather than $D_P D_{LM}$, is used, which leads to the following lemma:

Lemma 5.1. *The output of $D_{P(I)}D_{LM}$ satisfies: $\frac{\tilde{\mathbf{s}}^\top \tilde{\mathbf{s}}}{\tilde{\mathbf{s}}^\top \tilde{\mathbf{y}}} \leq \frac{1}{\mu_2}$, $\frac{\tilde{\mathbf{y}}^\top \tilde{\mathbf{y}}}{\tilde{\mathbf{s}}^\top \tilde{\mathbf{y}}} \leq \frac{1}{\mu_3}$, where $\mu_3 = \frac{\mu_1}{\mu_2(1+2\mu_1)}$.*

Consequently, one can prove the following two lemmas:

Lemma 5.2. *Suppose that we use (\mathbf{s}, \mathbf{y}) for the BFGS update (11). If $\frac{\mathbf{s}^\top \mathbf{s}}{\mathbf{s}^\top \mathbf{y}} \leq \frac{1}{\mu_2}$, $\frac{\mathbf{y}^\top \mathbf{y}}{\mathbf{s}^\top \mathbf{y}} \leq \frac{1}{\mu_3}$, then $\|B^+\| \leq \|B\| + \frac{1}{\mu_3}$ and $\|H^+\| \leq (1 + \frac{1}{\sqrt{\mu_2\mu_3}})^2 \|H\| + \frac{1}{\mu_2}$, where B denotes the inverse of H .*

Lemma 5.3. *In Algorithm 3, for a given layer index $l = 1, \dots, L$, there exist two positive constants $\underline{\kappa}_G^l$ and $\bar{\kappa}_G^l$, such that $\underline{\kappa}_G^l I \preceq H_G^l(k) \preceq \bar{\kappa}_G^l I, \forall k$.*

To apply the convergence results in Wang et al. (2017) to Algorithm 3, we need to have that H_A^l , and hence that $H_l = H_A^l \otimes H_G^l$, is bounded above and below by positive definite matrices, in addition to H_G^l . For this purpose and for satisfying other requirements needed to apply the theory in Wang et al. (2017), we make the following assumptions:

Assumption 5.4. $f : \mathbb{R}^d \rightarrow \mathbb{R}$ is continuously differentiable. $f(\theta)$ is lower bounded by a real number f^{low} for any $\theta \in \mathbb{R}^d$. ∇f is globally Lipschitz continuous with Lipschitz constant L , i.e., for any $\theta, \theta' \in \mathbb{R}^d$, $\|\nabla f(\theta) - \nabla f(\theta')\| \leq L\|\theta - \theta'\|$.

Assumption 5.5. For every iteration k , we have

$$\begin{aligned} a) \mathbb{E}_{\xi_k} [g(\theta_k, \xi_k)] &= \nabla f(\theta_k), \\ b) \mathbb{E}_{\xi_k} [\|g(x_k, \xi_k) - \nabla f(\theta_k)\|^2] &\leq \sigma^2, \end{aligned}$$

where g is the minibatch gradient and $\sigma > 0$ is the noise level of the gradient estimation, and $\xi_k, k = 1, 2, \dots$ are independent samples, and for a given k the random variable ξ_k is independent of $\{\theta_j\}_{j=1}^k$.

Assumption 5.6. The inputs $a_{j,t}^l$'s to any layers are bounded, i.e. $\exists \varphi > 0$ s.t. $\forall l, j, t, |a_{j,t}^l| \leq \varphi$.

Note that AS. 5.6 is relatively mild, in the sense that it is fulfilled if the activation functions of the model are all bounded (e.g. sigmoid, tanh, binary step), or some appropriate "normalization" is performed before the data are fed into each layer.

We now show that our block-diagonal approximation to Hessian is bounded below and above by positive definite matrices in Lemma 5.7, and after that, applying Theorem 2.8 in Wang et al. (2017) we obtain our main convergence result, Theorem 5.8. The complete proofs of all of the lemmas and the theorem in this section are deferred to Sec C.1 in the Appendix.

Lemma 5.7. *For Algorithm 3, under the assumption AS. 5.6, (i) $\hat{A}_l \preceq (J_l|\Delta|\varphi^2 + 1)|\mathcal{T}^l|I, \forall l$, and (ii) there exist two positive constants $\underline{\kappa}$ and $\bar{\kappa}$, such that $\underline{\kappa}I \preceq H = \text{diag}\{H_1, \dots, H_L\} \preceq \bar{\kappa}I$.*

Theorem 5.8. *Suppose that assumptions AS.5.4, AS.5.5, AS.5.6 hold for $\{\theta_k\}$ generated by Algorithm 3. We also assume that α_k is specifically chosen as $\alpha_k = \frac{\underline{\kappa}}{L\bar{\kappa}^2}k^{-\beta}$ with $\beta \in (0.5, 1)$. Then*

$$\begin{aligned} \frac{1}{K} \sum_{k=1}^K \mathbb{E} [\|\nabla f(\theta_k)\|^2] &\leq \frac{2L(M_f - f^{\text{low}})\bar{\kappa}^2}{\underline{\kappa}^2} K^{\beta-1} \\ &\quad + \frac{\sigma^2}{(1-\beta)m} (K^{-\beta} - K^{-1}), \end{aligned}$$

where K denotes the iteration number and M_f is a positive constant. Moreover, for a given $\epsilon \in (0, 1)$, to guarantee that $\frac{1}{K} \sum_{k=1}^K \mathbb{E} [\|\nabla f(\theta_k)\|^2] < \epsilon$, the number of iterations K needed is at most $O\left(\epsilon^{-\frac{1}{1-\beta}}\right)$.

Theorem 5.8 shows that Algorithm 3 converges to a stationary point for a (possibly) non-convex function f . We note that under very similar assumptions, Theorems 2.5 and 2.6 in Wang et al. (2017) also hold for Algorithm 3.

6. Numerical Results

In this section, we describe two sets of experiments, namely, three MLP autoencoder problems and four CNN problems, comparing our proposed methods to other relevant methods (see Sec D.1 for the detailed description of them) mentioned in our paper.

The results reported in the tables and plots are all based on runs using 5 different random seeds and the tuned best hyper-parameters (HPs) from a grid search specified below. The values reported in the tables and the solid curves depicted in the plots are derived from the averages of the 5 runs, while the shaded areas in the plots depict the $\pm\text{std}/\sqrt{5}$ range for the runs. All experiments were run on a machine with 8 Xeon Gold 6248 CPUs with one Nvidia V100 GPU.

6.1. Comparison with Goldfarb et al. (2020)

Our first set of experiments are on three MLP autoencoder problems with MNIST (LeCun et al., 1998), FACES, and CURVES (Hinton & Salakhutdinov, 2006) datasets, that have become standard for testing the performance of algorithms to train DNNs, (e.g., see Goldfarb et al. (2020)). We tested our proposed K-BFGS and K-BFGS(L) methods, their counterpart in Goldfarb et al. (2020) (i.e., K-BFGS-20 and K-BFGS(L)-20), as well as three SOTA methods, SGD with momentum (SGD-m), Adam, and KFAC. See Section D.2 in the Appendix for the model architecture and dataset details.

Minibatches of size 1000 were used for all three problems, as in Goldfarb et al. (2020). Each algorithm was run for a fixed amount of time for each problem (500 seconds for MNIST and CURVES, 2000 seconds for FACES). For all Kronecker-factored QN method, we set $T = 1$, except the one denoted as K-BFGS[†], which used $T = 20$. For KFAC, we set $T_1 = 1$ and $T_2 = 20$. These settings are exactly the same as those in Goldfarb et al. (2020).

As we are primarily interested in optimization performance in these experiments, we conducted a grid search on two hyper-parameters (HPs), namely, learning rate and damping, for all methods (only learning rate for SGD-m), and selected the best HP values that achieved the smallest loss on the training set. (See Section D.2 in the Appendix for the searching range and best HP values selected.) Finally, we ran each algorithm with their best HPs, using 5 different random seeds, and reported the average loss in Table 3. (See Figures 2 to 4 in the Appendix for the training curves.)

From Table 3, we can clearly see that K-BFGS and K-BFGS(L) consistently outperformed their counterparts in Goldfarb et al. (2020), justifying the effectiveness of the generic improvements we incorporated in K-BFGS. (See Sec D.2.1 in the Appendix for a more complete ablation study.) Moreover, K-BFGS and K-BFGS(L) also performed better than the 1st-order methods in most cases except for Adam on CURVES. Lastly, our proposed methods performed similarly to KFAC, particularly when amortization was used (see K-BFGS[†]). Note that the KFAC baseline that we implemented was better than the one in Goldfarb et al. (2020), since it splits the overall damping term adaptively (see Line 19 of Algorithm 5 in the Appendix), rather than simply setting $\pi_l = 1$, which turned out to be an important factor for KFAC.

Table 3. Average of training loss achieved using 5 different random seed with best HP values. The dagger sign (†) denotes that the curvature update frequency $T = 20$

	MNIST	FACES	CURVES
K-BFGS	51.60	5.00	55.46
K-BFGS [†]	52.01	4.62	55.06
K-BFGS(L)	51.53	4.83	55.31
K-BFGS-20	52.38	5.46	56.00
K-BFGS(L)-20	54.27	4.92	55.94
KFAC	51.33	4.75	54.84
Adam	52.76	5.33	55.24
SGD-m	54.75	6.47	55.97

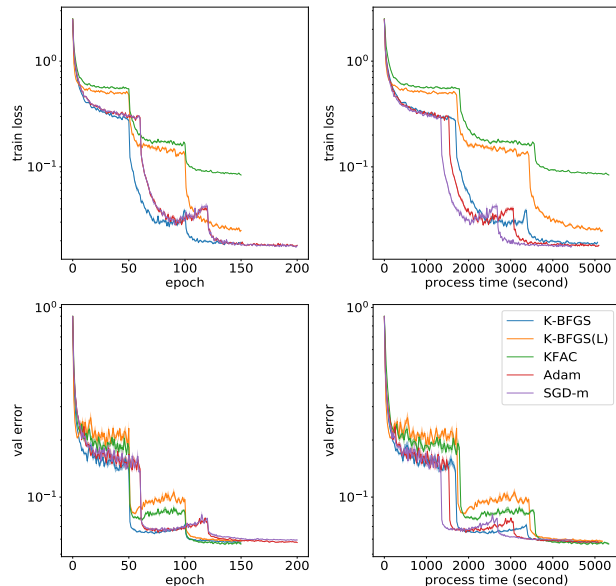


Figure 1. Training cross entropy loss (the upper row) and validation classification error (the lower row) against number of epochs (the left column) and process time (the right column) of K-BFGS, K-BFGS(L), KFAC, Adam, and SGD-m on VGG16 with CIFAR10.

6.2. CNNs: Generalization Performance

We tested K-BFGS, K-BFGS(L), KFAC, Adam, and SGD-m on two CNN models that have been found to be effective, namely, VGG16 (Simonyan & Zisserman, 2014) and ResNet32 (He et al., 2016). We experimented on both models, using two datasets, CIFAR-10 and CIFAR-100 (Krizhevsky et al., 2009), each of which includes 50,000 training samples and 10,000 testing samples (we view them as the validation set in our experiments). For both datasets, we applied the data augmentation techniques in Krizhevsky et al. (2012), including random horizontal flip and random crop. (See Sec D.3 in the Appendix for more details about the experimental set-up.) The above model/dataset choices have been used and endorsed in many papers, e.g. Zhang et al. (2019); Choi et al. (2019); Ren & Goldfarb (2021).

Minibatches of size 128 were used for all experiments. For SGD-m and Adam, we ran the algorithms for 200 epochs and decay the learning rate by a factor of 0.1 every 60 epochs, which has been shown to be an effective learning rate schedule for these 1st-order methods on these problems. For K-BFGS, K-BFGS(L), and KFAC, we ran the algorithms for 150 epochs and decay the learning rate by a factor of 0.1 every 50 epochs, so that their overall running time is approximately the same as that of the 1st-order methods. For K-BFGS, we set the curvature update frequency $T = 20$. For KFAC, we set $T_1 = 10$ and $T_2 = 100$, as in Zhang et al. (2019).

As we are interested in generalization performance in these experiments, we incorporated the weight decay technique (see Sec D.3 in the Appendix) and conducted a grid search on three hyper-parameters (HPs), namely, initial learning rate, weight decay factor, and damping for all methods (only initial learning rate and weight decay for SGD-m). Then, we selected HP values that achieved the largest classification accuracy on the validation set (the grid search ranges and the best HP values so

Table 4. Average of validation classification accuracy (%) achieved using 5 different random seeds with best HP values

Dataset Model	CIFAR10		CIFAR100	
	VGG16	ResNet32	VGG16	ResNet32
K-BFGS	94.28	93.45	75.65	71.46
KFAC	94.44	93.44	76.32	71.92
Adam	94.28	93.35	75.64	70.35
SGD-m	94.14	93.13	75.41	70.18

determined, are listed in Sec D.3 in the Appendix), and reported the average classification accuracy on the validation sets in Table 4. (See Figure 1 for the training and validation curves on VGG16+CIFAR10 and Figures 5, 6, and 7 in the Appendix for the others.)

Results in Table 4 indicate that K-BFGS² clearly outperformed Adam and SGD-m in terms of generalization, with the exception that K-BFGS and Adam achieved the same accuracy on VGG16+CIFAR10. Admittedly, KFAC achieved better accuracy than K-BFGS in 3 out of the 4 problems, but the gap is relatively small.

Finally, by comparing the process times reported in Figures 1 as well as Figures 5, 6, and 7 in the Appendix, we can see that the per-iteration time of K-BFGS is only about 1/3 more than it is for the 1st-order methods. Moreover, the per-iteration time of K-BFGS (with $T = 20$) is roughly the same as KFAC (with $T_2 = 100$), which demonstrates the effectiveness of our QN approach.

7. Conclusion

In this paper, we proposed a new class of Kronecker-factored quasi-Newton methods that are applicable to both MLP and CNN models, and that substantially improve upon the methods described in Goldfarb et al. (2020). We believe that our new methods are the first ones within the scope of quasi-Newton methods that use Kronecker-factored curvature approximations and are practical for training CNNs.

With extensive numerical experiments, our new methods are shown to be better than the ones in Goldfarb et al. (2020). On several standard CNN models, K-BFGS outperforms SOTA first-order methods and performs similarly to KFAC.

²Results in Table 4 do not include K-BFGS(L) because it consistently underperformed K-BFGS. See Figure 1 and Figures 5, 6, and 7 in the Appendix for K-BFGS(L) results.

References

- Amari, S.-I., Park, H., and Fukumizu, K. Adaptive method of realizing natural gradient learning for multilayer perceptrons. *Neural computation*, 12(6):1399–1409, 2000.
- Bakker, C., Henry, M. J., and Hodas, N. O. The outer product structure of neural network derivatives. *arXiv preprint arXiv:1810.03798*, 2018.
- Botev, A., Ritter, H., and Barber, D. Practical Gauss-Newton optimisation for deep learning. In *Proceedings of the 34th International Conference on Machine Learning-Volume 70*, pp. 557–565. JMLR. org, 2017.
- Broyden, C. G. The convergence of a class of double-rank minimization algorithms 1. general considerations. *IMA Journal of Applied Mathematics*, 6(1):76–90, 1970.
- Byrd, R. H., Nocedal, J., and Schnabel, R. B. Representations of quasi-Newton matrices and their use in limited memory methods. *Mathematical Programming*, 63(1-3):129–156, 1994.
- Byrd, R. H., Hansen, S. L., Nocedal, J., and Singer, Y. A stochastic quasi-Newton method for large-scale optimization. *SIAM Journal on Optimization*, 26(2):1008–1031, 2016.
- Choi, D., Shallue, C. J., Nado, Z., Lee, J., Maddison, C. J., and Dahl, G. E. On empirical comparisons of optimizers for deep learning. *arXiv preprint arXiv:1910.05446*, 2019.
- Duchi, J., Hazan, E., and Singer, Y. Adaptive subgradient methods for online learning and stochastic optimization. *Journal of Machine Learning Research*, 12(Jul):2121–2159, 2011.
- Fletcher, R. A new approach to variable metric algorithms. *The computer journal*, 13(3):317–322, 1970.
- George, T., Laurent, C., Bouthillier, X., Ballas, N., and Vincent, P. Fast approximate natural gradient descent in a Kronecker factored eigenbasis. In *Advances in Neural Information Processing Systems*, pp. 9550–9560, 2018.
- Goldfarb, D. A family of variable-metric methods derived by variational means. *Mathematics of computation*, 24(109): 23–26, 1970.
- Goldfarb, D., Ren, Y., and Bahamou, A. Practical quasi-Newton methods for training deep neural networks. In Larochelle, H., Ranzato, M., Hadsell, R., Balcan, M. F., and Lin, H. (eds.), *Advances in Neural Information Processing Systems*, volume 33, pp. 2386–2396. Curran Associates, Inc., 2020. URL <https://proceedings.neurips.cc/paper/2020/file/192fc044e74dffe144f9ac5dc9f3395-Paper.pdf>.
- Gower, R., Goldfarb, D., and Richtárik, P. Stochastic block BFGS: Squeezing more curvature out of data. In *International Conference on Machine Learning*, pp. 1869–1878, 2016.
- Grosse, R. and Martens, J. A Kronecker-factored approximate fisher matrix for convolution layers. In *International Conference on Machine Learning*, pp. 573–582, 2016.
- Gupta, V., Koren, T., and Singer, Y. Shampoo: Preconditioned stochastic tensor optimization. In Dy, J. and Krause, A. (eds.), *Proceedings of the 35th International Conference on Machine Learning*, volume 80 of *Proceedings of Machine Learning Research*, pp. 1842–1850. PMLR, 2018.
- He, K., Zhang, X., Ren, S., and Sun, J. Deep residual learning for image recognition. In *Proceedings of the IEEE conference on computer vision and pattern recognition*, pp. 770–778, 2016.
- Heskes, T. On "natural" learning and pruning in multilayered perceptrons. *Neural Computation*, 12, 01 2000. doi: 10.1162/089976600300015637.
- Hinton, G., Srivastava, N., and Swersky, K. Neural networks for machine learning lecture 6a overview of mini-batch gradient descent. *Cited on*, 14(8), 2012.
- Hinton, G. E. and Salakhutdinov, R. R. Reducing the dimensionality of data with neural networks. *science*, 313(5786): 504–507, 2006.

- Kingma, D. and Ba, J. Adam: A method for stochastic optimization. *International Conference on Learning Representations*, 2014.
- Krizhevsky, A., Hinton, G., et al. Learning multiple layers of features from tiny images. 2009.
- Krizhevsky, A., Sutskever, I., and Hinton, G. E. Imagenet classification with deep convolutional neural networks. In Pereira, F., Burges, C. J. C., Bottou, L., and Weinberger, K. Q. (eds.), *Advances in Neural Information Processing Systems*, volume 25, pp. 1097–1105. Curran Associates, Inc., 2012. URL <https://proceedings.neurips.cc/paper/2012/file/c399862d3b9d6b76c8436e924a68c45b-Paper.pdf>.
- LeCun, Y., Bottou, L., Bengio, Y., and Haffner, P. Gradient-based learning applied to document recognition. *Proceedings of the IEEE*, 86(11):2278–2324, 1998.
- Liu, D. C. and Nocedal, J. On the limited memory BFGS method for large scale optimization. *Mathematical programming*, 45(1-3):503–528, 1989.
- Loshchilov, I. and Hutter, F. Decoupled weight decay regularization. In *International Conference on Learning Representations*, 2019. URL <https://openreview.net/forum?id=Bkg6RiCqY7>.
- Martens, J. Deep learning via hessian-free optimization. In *ICML*, volume 27, pp. 735–742, 2010.
- Martens, J. and Grosse, R. Optimizing neural networks with Kronecker-factored approximate curvature. In *International conference on machine learning*, pp. 2408–2417, 2015.
- Martens, J., Ba, J., and Johnson, M. Kronecker-factored curvature approximations for recurrent neural networks. In *International Conference on Learning Representations*, 2018. URL <https://openreview.net/forum?id=HyMTkQZAb>.
- Povey, D., Zhang, X., and Khudanpur, S. Parallel training of dnns with natural gradient and parameter averaging. *arXiv preprint arXiv:1410.7455*, 2014.
- Ren, Y. and Goldfarb, D. Efficient subsampled Gauss-Newton and natural gradient methods for training neural networks. *arXiv preprint arXiv:1906.02353*, 2019.
- Ren, Y. and Goldfarb, D. Tensor normal training for deep learning models. In Beygelzimer, A., Dauphin, Y., Liang, P., and Vaughan, J. W. (eds.), *Advances in Neural Information Processing Systems*, 2021. URL <https://openreview.net/forum?id=-t9LPHRYKmi>.
- Robbins, H. and Monro, S. A stochastic approximation method. *The annals of mathematical statistics*, pp. 400–407, 1951.
- Shanno, D. F. Conditioning of quasi-Newton methods for function minimization. *Mathematics of computation*, 24(111): 647–656, 1970.
- Simonyan, K. and Zisserman, A. Very deep convolutional networks for large-scale image recognition. *arXiv preprint arXiv:1409.1556*, 2014.
- Vinyals, O. and Povey, D. Krylov subspace descent for deep learning. In *Artificial Intelligence and Statistics*, pp. 1261–1268, 2012.
- Wang, X., Ma, S., Goldfarb, D., and Liu, W. Stochastic quasi-Newton methods for nonconvex stochastic optimization. *SIAM Journal on Optimization*, 27(2):927–956, 2017.
- Wu, Y., Mansimov, E., Grosse, R. B., Liao, S., and Ba, J. Scalable trust-region method for deep reinforcement learning using Kronecker-factored approximation. *Advances in neural information processing systems*, 30:5279–5288, 2017.
- Wu, Y., Zhu, X., Wu, C., Wang, A., and Ge, R. Dissecting hessian: Understanding common structure of hessian in neural networks. *arXiv preprint arXiv:2010.04261*, 2020.
- Xu, P., Roosta, F., and Mahoney, M. W. Newton-type methods for non-convex optimization under inexact hessian information. *Mathematical Programming*, pp. 1–36, 2019.
- Zhang, G., Wang, C., Xu, B., and Grosse, R. Three mechanisms of weight decay regularization. In *International Conference on Learning Representations*, 2019. URL <https://openreview.net/forum?id=B1lz-3Rct7>.

A. Pseudo-code and Implementation Details for K-BFGS / K-BFGS(L)

A.1. Pseudo-code for K-BFGS / K-BFGS(L)

Algorithm 2 Pseudo-code for K-BFGS / K-BFGS(L)

Require: Given learning rates $\{\alpha_k\}$, damping value λ , curvature update frequency T , batch size m

- 1: $\mu_1 = 0.2, \beta = 0.9$
 - 2: $\lambda_A^l = \sqrt{|\mathcal{T}^l|}\sqrt{\lambda}, \lambda_G^l = \frac{1}{\sqrt{|\mathcal{T}^l|}}\sqrt{\lambda} \ (l = 1, \dots, L)$ $\{\mathcal{T}^l$ denotes the sets of spatial locations in layer $l\}$
 - 3: $\widetilde{\mathcal{D}W}_l = 0, A_l = \mathbb{E}_n [\sum_{t \in \mathcal{T}} \mathbf{a}_t^l(n) \mathbf{a}_t^l(n)^\top], H_A^l = (A_l + \lambda_A^l I_A)^{-1}, H_G^l = (\lambda_G^l)^{-1} I, \mathbf{s}_G^l = \mathbf{y}_G^l = 0 \ (l = 1, \dots, L)$
 $\{\text{Initialization}\}$
 - 4: **for** $k = 1, 2, \dots$ **do**
 - 5: Sample mini-batch M_k of size m
 - 6: Perform a forward-backward pass over M_k to compute stochastic gradient $\widetilde{\mathcal{D}W}_l \ (l = 1, \dots, L)$
 - 7: **for** $l = 1, \dots, L$ **do**
 - 8: $\widetilde{\mathcal{D}W}_l = \beta \widetilde{\mathcal{D}W}_l + \widetilde{\mathcal{D}W}_l$
 - 9: $p_l = H_G^l \widetilde{\mathcal{D}W}_l H_A^l$ $\{\text{if L-BFGS is used for } H_G^l, \text{ it is initialized as } \lambda_G^{-1} I\}$
 - 10: $W_l = W_l - \alpha_k p_l$
 - 11: **end for**
 - 12: **if** $k \equiv 0 \pmod{T}$ **then**
 - 13: Perform another forward-backward pass over M_k to compute $\overline{\mathbf{h}}_l^+$ and $\overline{\mathcal{D}h}_l^+ \ (l = 1, \dots, L)$
 - 14: **for** $l = 1, \dots, L$ **do**
 - 15: $\{\text{Update } H_A^l \text{ by BFGS}\}$
 - 16: $\mathbf{s}_A^l = H_A^l \widetilde{\mathbf{a}}_l, \mathbf{y}_A^l = \widetilde{A}_l \mathbf{s}_A^l + \lambda_A^l \mathbf{s}_A^l$ using (15)
 - 17: Use BFGS updating (11) with $(\mathbf{s}_A^l, \mathbf{y}_A^l)$ to update H_A^l
 - 18: $\{\text{Update } H_G^l \text{ by BFGS or L-BFGS}\}$
 - 19: $\mathbf{s}_G^l = \beta \mathbf{s}_G^l + (1 - \beta) \left(\widetilde{\mathbf{h}}_l^+ - \widetilde{\mathbf{h}}_l \right), \mathbf{y}_G^l = \beta \mathbf{y}_G^l + (1 - \beta) \left(\widetilde{\mathcal{D}h}_l^+ - \widetilde{\mathcal{D}h}_l \right).$
 - 20: $(\widetilde{\mathbf{s}}_G^l, \widetilde{\mathbf{y}}_G^l) = D_P D_{LM}(\mathbf{s}_G^l, \mathbf{y}_G^l)$ with $H = H_G^l, \mu_1 = \mu_1, \mu_2 = \lambda_G^l$ $\{\text{See Algorithm 1}\}$
 - 21: Use BFGS or L-BFGS with $(\widetilde{\mathbf{s}}_G^l, \widetilde{\mathbf{y}}_G^l)$ to update H_G^l $\{\text{We name the algorithm K-BFGS or K-BFGS(L), respectively, when BFGS or L-BFGS is used.}\}$
 - 22: **end for**
 - 23: **end if**
 - 24: **end for**
-

Algorithm 2 gives the pseudo-code for our proposed methods K-BFGS and K-BFGS(L). Note that one can use either BFGS or L-BFGS update for H_G , in which case we name the algorithm K-BFGS and K-BFGS(L), respectively. For simplicity, we assume that all layers in the model are convolutional layers. However, the algorithm can easily be adapted to fully-connected layers, hence applicable to MLP models or CNN models that contain fully-connected layers.

A.2. Usage of Minibatches and Moving Averages

Because there is usually a large amount of data, we use minibatches to estimate the quantities needed at every iteration. We use \widetilde{X} to denote the average value of X over a minibatch for any quantity X , which is usually used as an estimate to $\mathbb{E}_n[X(n)]$. Moreover, we use moving averages to both reduce the stochasticity and incorporate more information from the past:

- **Gradient.** At every iteration, the gradient $\widetilde{\mathcal{D}W}$ is estimated from a minibatch. We use a momentum scheme to get a better estimate $\widehat{\mathcal{D}W}$ of the gradient, i.e. we update

$$\widehat{\mathcal{D}W} = \beta \widehat{\mathcal{D}W} + \widetilde{\mathcal{D}W}.$$

- **BFGS updating for H_G .** By (12) and (13), we use both a minibatch and moving averages to estimate the (\mathbf{s}, \mathbf{y}) for H_G , i.e. we update

$$\begin{aligned}\mathbf{s}_G &= \beta \mathbf{s}_G + (1 - \beta) \left(\widetilde{\mathbf{h}^+} - \widetilde{\mathbf{h}} \right), \\ \mathbf{y}_G &= \beta \mathbf{y}_G + (1 - \beta) \left(\widetilde{\mathcal{D}\mathbf{h}^+} - \widetilde{\mathcal{D}\mathbf{h}} \right).\end{aligned}$$

- **BFGS updating for H_A .** In (14), we estimate the value of A from the current minibatch, i.e. $\widetilde{\sum_{t \in \mathcal{T}} A_{t,t}}$, as well as $\hat{\mathbf{a}} = \widetilde{\mathbf{a}}$. Note that A_{s_A} can be computed without forming A .

A.3. Other Details

Unlike Goldfarb et al. (2020), which always perform the whole K-BFGS process at every iteration, we introduce the so-called curvature update frequency T , controlling how frequently the algorithm update its curvature matrices. In other words, when $k \not\equiv 0 \pmod{T}$, only from Line 5 to Line 11 of Algorithm 2 is incurred.

Note that Algorithm 2 contains only one damping hyper-parameter (HP) λ , and sets $\lambda_A^l = \sqrt{|\mathcal{T}^l|} \sqrt{\lambda}$, $\lambda_G^l = \frac{1}{\sqrt{|\mathcal{T}^l|}} \sqrt{\lambda}$ for each convolutional layer $l = 1, \dots, L$, where \mathcal{T}^l denotes the sets of spatial locations in layer l . This can be viewed as "rebalancing" A and G , i.e. setting A to be $\mathbb{E}_n \left[\frac{1}{\sqrt{|\mathcal{T}^l|}} \sum_{t \in \mathcal{T}} A_{t,t}(n) \right]$ and G to be $\mathbb{E}_n \left[\frac{1}{\sqrt{|\mathcal{T}^l|}} \sum_{t \in \mathcal{T}} G_{t,t}(n) \right]$. For fully-connected layers (if there is any), we set $\lambda_A^l = \lambda_G^l = \sqrt{\lambda}$, as in Goldfarb et al. (2020). Since $\lambda_A^l \lambda_G^l = \lambda$, adding $\lambda_A^l \mathbf{s}_A^l$ and $\lambda_G^l \mathbf{s}_G^l$, respectively, to the vectors \mathbf{y}_A^l and \mathbf{y}_G^l before applying BFGS (or L-BFGS) to H_A^l and H_G^l , can be viewed as an approximation to adding the overall LM damping factor λI to $(H^l)^{-1} = (H_A^l)^{-1} \otimes (H_G^l)^{-1}$ prior to updating.

Moreover, a warm start computation of A_l is included, i.e. A_l is computed from the whole dataset before first iteration, which is then used to initialize H_A^l . This only introduces a mild overhead, as this warm start computation take no more than the time for one full epoch, and gives a good starting point of H_A^l .

When using the L-BFGS derived matrix H_G^l to compute $H_G^l \widehat{\mathcal{D}\mathbf{W}_l}$, instead of using the classical two-loop recursion of L-BFGS, we follow the "non-loop" implementation in Byrd et al. (1994), which is faster in practice because $\widehat{\mathcal{D}\mathbf{W}_l}$ is a matrix, not a vector.

For CNN models that have batch normalization layers, we use the momentum gradient directions to update its parameters, with its own learning rate α_k/λ . (Note that α_k/λ can be viewed as the "effective" learning rate in K-BFGS, roughly speaking.)

In terms of some default hyper-parameters, as shown in Algorithm 2, decay parameters $\beta = 0.9$, and $\mu_1 = 0.2$ in $D_F D_{LM}$. For K-BFGS(L), the number of (\mathbf{s}, \mathbf{y}) pairs stored for L-BFGS was set to be 100. These settings are exactly the same as in Goldfarb et al. (2020).

B. Proof of Theorem 2.1

Proof. We first derive the structure of the gradient. By (1),

$$\begin{aligned}\frac{\partial f}{\partial w_{i,j,\delta}} &= \sum_{t \in \mathcal{T}} \frac{\partial f}{\partial h_{i,t}} \frac{\partial h_{i,t}}{\partial w_{i,j,\delta}} = \sum_{t \in \mathcal{T}} \mathcal{D}h_{i,t} a_{j,t+\delta}, \\ \frac{\partial f}{\partial b_i} &= \sum_{t \in \mathcal{T}} \frac{\partial f}{\partial h_{i,t}} \frac{\partial h_{i,t}}{\partial b_i} = \sum_{t \in \mathcal{T}} \mathcal{D}h_{i,t}.\end{aligned}$$

Hence,

$$\mathcal{D}\mathbf{w}_i = \sum_{t \in \mathcal{T}} \mathcal{D}h_{i,t} \mathbf{a}_t \Rightarrow \mathcal{D}\mathbf{W} = \sum_{t \in \mathcal{T}} \mathcal{D}\mathbf{h}_t (\mathbf{a}_t)^\top.$$

and $\text{vec}(\mathcal{D}\mathbf{W}) = \sum_{t \in \mathcal{T}} \mathbf{a}_t \otimes \mathcal{D}\mathbf{h}_t$.

To derive the Hessian of $f(\cdot; \theta)$ for a single data-point, it follows from (1) that

$$\begin{aligned}\frac{\partial(\mathcal{D}h_{i,t})}{\partial w_{i',j,\delta}} &= \sum_{t'} \frac{\partial(\mathcal{D}h_{i,t})}{\partial h_{i',t'}} \frac{\partial h_{i',t'}}{\partial w_{i',j,\delta}} = \sum_{t'} \frac{\partial^2 f}{\partial h_{i,t} \partial h_{i',t'}} a_{j,t'+\delta}, \\ \frac{\partial(\mathcal{D}h_{i,t})}{\partial b_{i'}} &= \sum_{t'} \frac{\partial(\mathcal{D}h_{i,t})}{\partial h_{i',t'}} \frac{\partial h_{i',t'}}{\partial b_{i'}} = \sum_{t'} \frac{\partial^2 f}{\partial h_{i,t} \partial h_{i',t'}}.\end{aligned}$$

Hence,

$$\frac{\partial(\mathcal{D}h_{i,t})}{\partial \mathbf{w}_{i'}} = \sum_{t'} \frac{\partial^2 f}{\partial h_{i,t} \partial h_{i',t'}} \mathbf{a}_{t'},$$

and

$$\frac{\partial^2 f}{\partial \mathbf{w}_i \partial \mathbf{w}_{i'}} = \frac{\partial}{\partial \mathbf{w}_{i'}} \left(\sum_t \mathcal{D}h_{i,t} \mathbf{a}_t \right) = \sum_t \frac{\partial(\mathcal{D}h_{i,t})}{\partial \mathbf{w}_{i'}} \mathbf{a}_t^\top = \sum_t \sum_{t'} \frac{\partial^2 f}{\partial h_{i,t} \partial h_{i',t'}} A_{t,t'}.$$

Hence,

$$\frac{\partial^2 f}{\partial \text{vec}(W)^2} = \sum_{t,t'} A_{t,t'} \otimes G_{t,t'}.$$

□

C. Proof of Convergence for a Variant of K-BFGS(L) and Associated Lemmas

Algorithm 3 K-BFGS(L) with $D_{P(I)}D_{LM}$ and exact inversion of A

Require: Given learning rates $\{\alpha_k\}$, damping values $\lambda_A^l, \lambda_G^l > 0$ ($l = 1, \dots, L$), batch size m , $0 < \mu_1 < 1$, $0 < \beta < 1$

- 1: $A_l = \mathbb{E}_n [\sum_{t \in \mathcal{T}} \mathbf{a}_t^l(n) \mathbf{a}_t^{l\top}(n)]$, $H_A^l = (A_l + \lambda_A^l I_A)^{-1}$, $H_G^l = (\lambda_G^l)^{-1} I$, $\mathbf{s}_G^l = \mathbf{y}_G^l = \mathbf{0}$ ($l = 1, \dots, L$) {Initialization}
- 2: **for** $k = 1, 2, \dots$ **do**
- 3: Sample mini-batch M_k of size m
- 4: Perform a forward-backward pass over M_k to compute stochastic gradient $\widetilde{\mathcal{D}W}_l$ ($l = 1, \dots, L$)
- 5: **for** $l = 1, \dots, L$ **do**
- 6: $p_l = H_G^l \widetilde{\mathcal{D}W}_l H_A^l$ { H_G^l is initialized as $\lambda_G^{-1} I$ in L-BFGS}
- 7: $W_l = W_l - \alpha_k p_l$
- 8: **end for**
- 9: Perform another forward-backward pass over M_k to compute $\overline{\mathbf{h}}_l^+$ and $\overline{\mathcal{D}\mathbf{h}}_l^+$ ($l = 1, \dots, L$)
- 10: **for** $l = 1, \dots, L$ **do**
- 11: {Compute H_A^l }
- 12: Compute $\hat{A}_l = \widetilde{\sum}_t A_{t,t}^l$, $H_A^l = (\hat{A}_l + \lambda_A^l I)^{-1}$
- 13: {Update H_G^l by L-BFGS}
- 14: $\mathbf{s}_G^l = \beta \mathbf{s}_G^l + (1 - \beta) \left(\overline{\mathbf{h}}_l^+ - \widetilde{\mathbf{h}}_l \right)$, $\mathbf{y}_G^l = \beta \mathbf{y}_G^l + (1 - \beta) \left(\overline{\mathcal{D}\mathbf{h}}_l^+ - \widetilde{\mathcal{D}\mathbf{h}}_l \right)$.
- 15: $(\widetilde{\mathbf{s}}_G^l, \widetilde{\mathbf{y}}_G^l) = D_{P(I)}D_{LM}(\mathbf{s}_G^l, \mathbf{y}_G^l)$ with $H = H_G^l$, $\mu_1 = \mu_1$, $\mu_2 = \lambda_G^l$ {See Algorithm 4}
- 16: Use L-BFGS with $(\widetilde{\mathbf{s}}_G^l, \widetilde{\mathbf{y}}_G^l)$ to update H_G^l
- 17: **end for**
- 18: **end for**

Algorithm 3 gives the variant of K-BFGS(L) that is used in the convergence proof. Algorithm 3 differs from the actual implementation of K-BFGS(L), i.e. the one in Algorithm 2, in the following:

1. $D_{P(I)}D_{LM}$ (Algorithm 4) is used instead of $D_P D_{LM}$ (Algorithm 1). $D_{P(I)}D_{LM}$ differs from $D_P D_{LM}$ by replacing H by a scaled identity matrix $\mu_2^{-1} I$, where it appears in Algorithm 1. This is justifiable partly because, in our actual implementation of L-BFGS, H_G is always initialized with the scaled identity matrix $\mu_2^{-1} I$ where $\mu_2 = \lambda_G^l$;

Algorithm 4 $D_{P(I)}D_{LM}$

```

1: Input:  $\mathbf{s}, \mathbf{y}$ ; Output:  $\tilde{\mathbf{s}}, \tilde{\mathbf{y}}$ ; Given:  $0 < \mu_1 < 1, \mu_2 > 0$ 
2: if  $\mathbf{s}^\top \mathbf{y} < \mu_1 \mathbf{y}^\top (\mu_2^{-1} I) \mathbf{y}$  then
3:    $\theta_1 = \frac{(1-\mu_1) \mathbf{y}^\top \mathbf{y} / \mu_2}{\mathbf{y}^\top \mathbf{y} / \mu_2 - \mathbf{s}^\top \mathbf{y}}$ 
4: else
5:    $\theta_1 = 1$ 
6: end if
7:  $\tilde{\mathbf{s}} = \theta_1 \mathbf{s} + (1 - \theta_1) \mu_2^{-1} \mathbf{y}$  {Powell's damping with  $H = \mu_2^{-1} I$ }
8:  $\tilde{\mathbf{y}} = \mathbf{y} + \mu_2 \tilde{\mathbf{s}}$  {Levenberg-Marquardt damping on  $H^{-1}$ }
9: return:  $\tilde{\mathbf{s}}, \tilde{\mathbf{y}}$ 
    
```

2. H_A^l is computed by simply inverting $\hat{A}_l + \lambda_A^l I$, instead of using minibatched Hessian-action BFGS;
3. Gradient is estimated from the current minibatch without momentum.

For simplicity, we also assume the curvature update frequency $T = 1$ in Algorithm 3. However, all the proofs and results still hold if $T > 1$.

C.1. Relevant Proofs for Theorem 5.8
C.1.1. PROOF OF LEMMA 5.1

Proof. First, similar to Powell's damping on H , we can show that $\tilde{\mathbf{s}}^\top \mathbf{y} \geq \frac{\mu_1}{\mu_2} \mathbf{y}^\top \mathbf{y} \geq 0$. Hence, $\tilde{\mathbf{s}}^\top \tilde{\mathbf{y}} = \tilde{\mathbf{s}}^\top \mathbf{y} + \mu_2 \tilde{\mathbf{s}}^\top \tilde{\mathbf{s}} \geq \mu_2 \tilde{\mathbf{s}}^\top \tilde{\mathbf{s}}$.

To see the second inequality, by using that $\tilde{\mathbf{s}}^\top \tilde{\mathbf{y}} \geq \tilde{\mathbf{s}}^\top \mathbf{y}$ it follows that

$$\begin{aligned} \tilde{\mathbf{y}}^\top \tilde{\mathbf{y}} &= \mathbf{y}^\top \mathbf{y} + 2\mu_2 \tilde{\mathbf{s}}^\top \mathbf{y} + \mu_2^2 \tilde{\mathbf{s}}^\top \tilde{\mathbf{s}} = \mathbf{y}^\top \mathbf{y} + 2\mu_2 \tilde{\mathbf{s}}^\top (\tilde{\mathbf{y}} - \mu_2 \mathbf{s}) + \mu_2^2 \tilde{\mathbf{s}}^\top \tilde{\mathbf{s}} \\ &\leq \mathbf{y}^\top \mathbf{y} + 2\mu_2 \tilde{\mathbf{s}}^\top \tilde{\mathbf{y}} \leq \mu_2 \left(\frac{1}{\mu_1} + 2 \right) \tilde{\mathbf{s}}^\top \tilde{\mathbf{y}}. \end{aligned}$$

□

C.1.2. PROOF OF LEMMA 5.2

Proof. Corresponding to the BFGS update (11) of H , the update of B is

$$B^+ = B - \frac{B \mathbf{s} \mathbf{s}^\top B}{\mathbf{s}^\top B \mathbf{s}} + \rho \mathbf{y} \mathbf{y}^\top.$$

Hence,

$$\|B^+\| \leq \|B - \frac{B \mathbf{s} \mathbf{s}^\top B}{\mathbf{s}^\top B \mathbf{s}}\| + \|\rho \mathbf{y} \mathbf{y}^\top\| \leq \|B\| + \frac{\mathbf{y}^\top \mathbf{y}}{\mathbf{s}^\top \mathbf{y}} \leq \|B\| + \frac{1}{\mu_3}.$$

Also, using the fact that for the spectral norm $\|\cdot\|$, $\|I - \rho \mathbf{s} \mathbf{y}^\top\| = \|I - \rho \mathbf{y} \mathbf{s}^\top\|$, we have that

$$\|H^+\| \leq \|H\| \|I - \rho \mathbf{s} \mathbf{y}^\top\|^2 + \left\| \frac{\mathbf{s} \mathbf{s}^\top}{\mathbf{s}^\top \mathbf{y}} \right\| \leq \|H\| \left(\|I\| + \frac{\|\mathbf{s}\| \|\mathbf{y}\|}{\mathbf{s}^\top \mathbf{y}} \right)^2 + \frac{\mathbf{s}^\top \mathbf{s}}{\mathbf{s}^\top \mathbf{y}} \leq \left(1 + \frac{1}{\sqrt{\mu_2}} \frac{1}{\sqrt{\mu_3}} \right)^2 \|H\| + \frac{1}{\mu_2}.$$

□

C.1.3. PROOF OF LEMMA 5.3

Proof. To simplify notation, we omit the subscript G , superscript l and the iteration index k in the proof. Hence, our goal is to prove $\underline{\kappa}_G I \preceq H = H_G^l(k) \preceq \bar{\kappa}_G I$, for any k . Let $(\mathbf{s}_i, \mathbf{y}_i)$ ($i = 1, \dots, p$) denote the pairs used in an L-BFGS computation of H .

Given an initial estimate $H_0 = B_0^{-1} = \lambda_G^{-1} I$ of $(G_l(\theta_k))^{-1}$, the L-BFGS method updates H_i recursively as

$$H_i = (I - \rho_i \mathbf{s}_i \mathbf{y}_i^\top) H_{i-1} (I - \rho_i \mathbf{y}_i \mathbf{s}_i^\top) + \rho_i \mathbf{s}_i \mathbf{s}_i^\top, \quad (16)$$

where $\rho_i = (\mathbf{s}_i^\top \mathbf{y}_i)^{-1}$, $i = 1, \dots, p$, and equivalently,

$$B_i = B_{i-1} - \frac{B_{i-1} \mathbf{s}_i \mathbf{s}_i^\top B_{i-1}}{\mathbf{s}_i^\top B_{i-1} \mathbf{s}_i} + \rho_i \mathbf{y}_i \mathbf{y}_i^\top, \quad i = 1, \dots, p,$$

where $B_i = H_i^{-1}$. Since we use $D_{P(I)} D_{LM}$, by Lemma 5.1, we have that $\frac{\mathbf{s}_i^\top \mathbf{s}_i}{\mathbf{s}_i^\top \mathbf{y}_i} \leq \frac{1}{\mu_2}$ and $\frac{\mathbf{y}_i^\top \mathbf{y}_i}{\mathbf{s}_i^\top \mathbf{y}_i} \leq \frac{1}{\mu_3}$.

Hence, by Lemma 5.2, we have that $\|B_i\| \leq \|B_{i-1}\| + \frac{1}{\mu_3}$. Hence, $\|B\| = \|B_p\| \leq \|B_0\| + \frac{p}{\mu_3} = \lambda_G + \frac{p}{\mu_3}$. Thus, $B \preceq \left(\lambda_G + \frac{p}{\mu_3}\right) I$, and $H \succeq \left(\lambda_G + \frac{p}{\mu_3}\right)^{-1} I \equiv \underline{\kappa}_G I$.

On the other hand, by Lemma 5.2, we have that $\|H_i\| \leq (1 + \frac{1}{\sqrt{\mu_2 \mu_3}})^2 \|H_{i-1}\| + \frac{1}{\mu_2}$. Hence, from the fact that $H_0 = \lambda_G^{-1} I$, and induction, we have that $\|H\| \leq \lambda_G^{-1} \hat{\mu}^p + \frac{\hat{\mu}^p - 1}{\hat{\mu} - 1} \frac{1}{\mu_2} \equiv \bar{\kappa}_G$, where $\hat{\mu} = (1 + \frac{1}{\sqrt{\mu_2 \mu_3}})^2$. □

C.1.4. PROOF OF LEMMA 5.7

Proof. In proving part (i), we omit the layer index l for simplicity. First, because \hat{A} is the averaged value across the minibatch, it suffices to show that for any data-point n , $\sum_t A_{t,t}(n) \preceq (J|\Delta|\varphi^2 + 1)|\mathcal{T}|I$.

By AS. 5.6, $\|\mathbf{a}_t(n)\|^2 = \sum_{j,\delta} a_{j,t+\delta}(n)^2 + 1 \leq J|\Delta|\varphi^2 + 1$. Hence, for any vector \mathbf{x} ,

$$\mathbf{x}^\top A_{t,t}(n) \mathbf{x} = \mathbf{x}^\top (\mathbf{a}_t(n) \mathbf{a}_t(n)^\top) \mathbf{x} = (\mathbf{a}_t(n)^\top \mathbf{x})^2 \leq \|\mathbf{a}_t(n)\|^2 \|\mathbf{x}\|^2 \leq (J|\Delta|\varphi^2 + 1) \|\mathbf{x}\|^2.$$

Hence, $A_{t,t}(n) \preceq (J|\Delta|\varphi^2 + 1)I$ and $\sum_t A_{t,t}(n) \preceq (J|\Delta|\varphi^2 + 1)|\mathcal{T}|I$, proving part (i).

Note that $\hat{A}_l + \lambda_A^l I \succeq \lambda_A^l I$ because \hat{A}_l is PSD. On the other hand, $\hat{A}_l + \lambda_A^l I \preceq ((J_l|\Delta|\varphi^2 + 1)|\mathcal{T}^l| + \lambda_A^l)I$. Hence,

$$((J_l|\Delta|\varphi^2 + 1)|\mathcal{T}^l| + \lambda_A^l)^{-1} I \preceq H_A^l = (\hat{A}_l + \lambda_A^l I)^{-1} \preceq (\lambda_A^l)^{-1} I. \quad (17)$$

By (17) and Lemma 5.3, we have that $\underline{\kappa}^l I \preceq H_A^l \otimes H_G^l = H_l \preceq \bar{\kappa}^l I$ where $\underline{\kappa}^l = ((J_l|\Delta|\varphi^2 + 1)|\mathcal{T}^l| + \lambda_A^l)^{-1} \underline{\kappa}_G^l$, $\bar{\kappa}^l = (\lambda_A^l)^{-1} \bar{\kappa}_G^l$. Finally, $\underline{\kappa} I \preceq H = \text{diag}\{H_1, \dots, H_L\} \preceq \bar{\kappa} I$, where $\underline{\kappa} = \min\{\underline{\kappa}^1, \dots, \underline{\kappa}^L\}$ and $\bar{\kappa} = \max\{\bar{\kappa}^1, \dots, \bar{\kappa}^L\}$. □

C.1.5. PROOF OF THEOREM 5.8

Proof. First, Algorithm 3 falls in the general framework of the Stochastic Quasi-Newton (SQN) method (Algorithm 2.1) in Wang et al. (2017). Second, by Lemma 5.7, Assumption AS.3 in Wang et al. (2017) is satisfied. Also, by the way H_A and H_G are updated, AS.4 in Wang et al. (2017) is satisfied. Hence, since Assumptions AS.1 and AS.2 are identical to the other two assumptions made in Wang et al. (2017), we are able to apply Theorem 2.8 in that paper to Algorithm 3 in this Section. □

D. Experiment Details

D.1. Specification on Comparing Algorithms

Algorithm 5 KFAC

Require: Given learning rates $\{\alpha_k\}$, damping value λ , batch size m , statistics update frequency T_1 , inverse update frequency T_2

- 1: $\beta = 0.9$
- 2: $\widehat{\mathcal{D}W}_l = 0$, $\Omega_l = \mathbb{E}_n [\sum_{t \in \mathcal{T}} \mathbf{a}_t^l(n) \mathbf{a}_t^l(n)^\top]$, $\Gamma_l = \mathbb{E}_n [\overline{\mathcal{D}h^l(n) (\mathcal{D}h^l(n))^\top}]$ with y sampled from the predictive distribution ($l = 1, \dots, L$) {Initialization}
- 3: **for** $k = 1, 2, \dots$ **do**
- 4: Sample minibatch M_k of size m
- 5: Perform a forward-backward pass over the current minibatch M_k to compute $\widetilde{\mathcal{D}W}_l$ for $l = 1, \dots, L$
- 6: **for** $l = 1, 2, \dots, L$ **do**
- 7: $\widehat{\mathcal{D}W}_l = \beta \widehat{\mathcal{D}W}_l + \widetilde{\mathcal{D}W}_l$
- 8: $p_l = H_\Gamma^l \widehat{\mathcal{D}W}_l H_\Omega^l$
- 9: $W_l = W_l - \alpha_k p_l$.
- 10: **end for**
- 11: **if** $k \equiv 0 \pmod{T_1}$ **then**
- 12: Perform another pass over M_k with y sampled from the predictive distribution to compute $\mathcal{D}h_t^l$ for $l = 1, \dots, L$
- 13: **for** $l = 1, 2, \dots, L$ **do**
- 14: Update $\Omega_l = \beta \cdot \Omega_l + (1 - \beta) \cdot \sum_{t \in \mathcal{T}} \widetilde{\mathbf{a}}_t^l (\widetilde{\mathbf{a}}_t^l)^\top$, $\Gamma_l = \beta \cdot \Gamma_l + (1 - \beta) \cdot \overline{\mathcal{D}h_t^l (\mathcal{D}h_t^l)^\top}$
- 15: **end for**
- 16: **end if**
- 17: **if** $k \equiv 0 \pmod{T_2}$ **then**
- 18: **for** $l = 1, 2, \dots, L$ **do**
- 19: Recompute $H_\Omega^l = (\Omega_l + \pi_l \sqrt{\lambda} I)^{-1}$, $H_\Gamma^l = (\Gamma_l + \frac{1}{\pi_l} \sqrt{\lambda} I)^{-1}$, where $\pi_l = \sqrt{\frac{\text{trace}(\Omega_l \otimes I)}{\text{trace}(I \otimes \Gamma_l)}}$
- 20: **end for**
- 21: **end if**
- 22: **end for**

We describe the version of KFAC that we implemented in Algorithm 5. Note that Ω_l in KFAC is the same as A_l in K-BFGS. Similar to the pseudo-code of K-BFGS, we assume that all layers are convolutional. However, one can easily derive our KFAC implementation for fully-connected layers from Algorithm 5 and Martens & Grosse (2015).

Note that KFC-pre in Grosse & Martens (2016) differs from Algorithm 5 in the following ways:

- KFC-pre uses clipping for the approximated natural gradient direction p ;
- KFC-pre uses momentum for p ;
- KFC-pre uses parameter averaging on θ .

All of these techniques can also be applied to K-BFGS. Since we are primarily interested in comparing different preconditioning matrices, we chose not to include such techniques in our implementation.

In our KFAC implementation, for the CNN problems that have batch normalization (BN) layers, we update the parameters of the BN layers with the gradient direction, along with the same learning rate α , as was done in Zhang et al. (2019).

Also note that in Algorithm 5, a warm start computation of Ω_l and Γ_l is included, i.e. initial estimates of Ω_l and Γ_l are computed from the whole dataset before the first iteration. A similar warm start computation of A_l was also included in K-BFGS. Since these warm start computations take no more than the time for one full epoch, we did not include the times for warm starts in the figures.

Finally, Adam was implemented exactly as in Kingma & Ba (2014), with $\beta_1 = 0.9$ and $\beta_2 = 0.999$, as suggested in the paper. We view the hyper-parameter ϵ in Adam as the damping term, and tune it in our experiments (specified below).

In SGD with momentum, the momentum of gradient is computed as in K-BFGS (Algorithm 2) and KFAC (Algorithm 5). In

Table 5. Model architectures for the MLP autoencoder problems

	Layer width	Loss function
MNIST	[784, 1000, 500, 250, 30, 250, 500, 1000, 784]	binary cross entropy with sigmoid
FACES	[625, 2000, 1000, 500, 30, 500, 1000, 2000, 625]	mean squared error
CURVES	[784, 400, 200, 100, 50, 25, 6, 25, 50, 100, 200, 400, 784]	binary cross entropy with sigmoid

 Table 6. Best HP values (learning rate, damping) for Table 3 as well as Figures 2, 3, and 4. The dagger sign (\dagger) denotes that the curvature update frequency $T = 20$

	K-BFGS	K-BFGS †	K-BFGS(L)	K-BFGS-20	K-BFGS(L)-20	KFAC	Adam	SGD-m
MNIST	(0.03, 0.3)	(0.3, 30)	(0.03, 0.3)	(0.01, 0.1)	(0.003, 0.1)	(0.3, 10)	(1e-4, 1e-4)	(0.003, -)
FACES	(0.03, 1)	(0.03, 3)	(0.03, 1)	(0.01, 0.3)	(0.01, 0.3)	(0.03, 0.1)	(1e-4, 1e-4)	(0.001, -)
CURVES	(0.03, 0.3)	(0.3, 30)	(0.1, 3)	(0.01, 0.03)	(0.003, 0.03)	(0.3, 10)	(1e-3, 1e-3)	(0.003, -)

other words, if g denotes the minibatch gradient, we update the momentum of gradient by $\hat{g} = \beta \hat{g} + g$ with $\beta = 0.9$ at every iteration.

D.2. Details on the Autoencoder Experiments

The autoencoder architectures are exactly the same as in Goldfarb et al. (2020). The only difference is that we didn’t include the regularization term $\frac{\eta}{2} \|\theta\|^2$, because we focus on optimization performance so it is better to avoid this compounding factor and it is hard to know how to set the value of η unless we include it in the HP tuning process. To be more specific, Table 5 describes the model architectures. The activation functions of the hidden layers are always ReLU, except that there is no activation for the very middle layer.

As in Goldfarb et al. (2020), we only use the training sets of the datasets, which contains 60k (MNIST³), 103.5k (FACES⁴), and 20k (CURVES⁵) training samples, respectively.

In order to obtain the results in Table 3, we first conducted a grid search for each algorithm based on the following ranges:

- learning rate: $\{ 3e-5, 1e-4, 3e-4, 1e-3, 3e-3, 0.01, 0.03, 0.1, 0.3, 1 \}$;
- damping:
 - Kronecker-factored QN methods (i.e., λ in Algorithm 2) and KFAC (i.e., λ in Algorithm 5): $\{ 0.03, 0.1, 0.3, 1, 3, 10, 30 \}$;
 - Adam (i.e., the ϵ HP in Kingma & Ba (2014)): $\{ 1e-8, 1e-4, 1e-3, 0.01, 0.1 \}$.

We selected the HP values that achieves the smallest training loss (see Table 6). We then ran each algorithm with their corresponding best HP values and 5 different random seed, and reported the average loss in Table 3. The training curves are also included in Figures 2, 3, and 4, where the training loss is reported against number of epochs (left) and process time (right).

³<http://yann.lecun.com/exdb/mnist/>

⁴http://www.cs.toronto.edu/~jmartens/newfaces_rot_single.mat

⁵http://www.cs.toronto.edu/~jmartens/digs3pts_1.mat

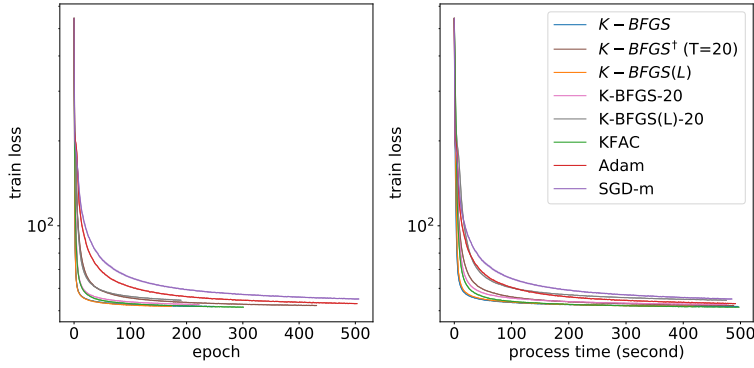


Figure 2. Optimization performance of K-BFGS, K-BFGS(L), their counterpart in Goldfarb et al. (2020), KFAC, Adam, and SGD-m on MNIST

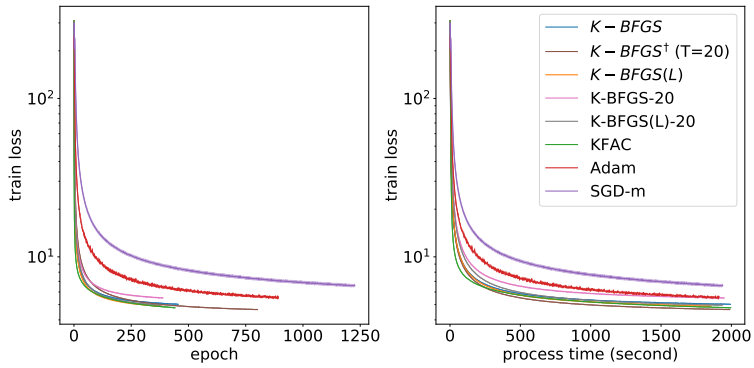


Figure 3. Optimization performance of K-BFGS, K-BFGS(L), their counterpart in Goldfarb et al. (2020), KFAC, Adam, and SGD-m on FACES

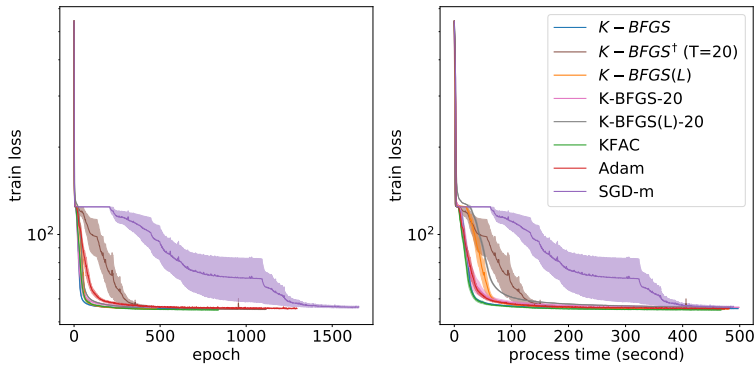


Figure 4. Optimization performance of K-BFGS, K-BFGS(L), their counterpart in Goldfarb et al. (2020), KFAC, Adam, and SGD-m on CURVES

D.2.1. AN ABLATION STUDY

Besides the comparison presented in Section 6.1, we also conducted an ablation study on the two generic improvements we presented in Section 3.2.1. To be more specific, if both of the improvements are turned on, the algorithm is exactly the same as the one named "K-BFGS" in Table 3, whereas if both are turned off, it is the same as "K-BFGS-20" in Table 3.

Table 7. Training loss with two improvements turned on or off. Reported values are averaged across 5 different random seeds, using the best HP values for each algorithm. Improvement #1 refers to the use of $D_F D_{LM}$, whereas improvement #2 refers to the use of "minibatched" Hessian-action BFGS

Name of algorithm	Improvement #1	Improvement #2	MNIST	FACES	CURVES
K-BFGS	yes	yes	51.60	5.00	55.46
K-BFGS (#1 off)	no	yes	51.92	5.39	55.86
K-BFGS (#2 off)	yes	no	51.45	5.26	55.88
K-BFGS-20	no	no	52.38	5.46	56.00

We repeated the same MLP autoencoder experiments described in Section 6.1, and presented the results on four different variants in Table 7, which shows that using each one of the improvements alone yields better results than the variant without improvements (i.e. K-BFGS-20), and using the two together (i.e. K-BFGS) usually yields the best results. This ablation study, along with the reasoning in Section 3.2.1, justifies the inclusion of the improvements we proposed.

D.3. Details on the CNN Experiments

The VGG16 model refers to the "model D" in [Simonyan & Zisserman \(2014\)](#), with the modifications that the 3 fully-connected (FC) layers at the end of the model being replaced with only one FC layer (input size equal the size of the output size of the last conv layer, and output size equal number of classes of the dataset), and a batch normalization layer is added after each of the convolutional layers in the model. These changes are usually adopted nowadays on top of the original VGG models. The ResNet32 model refers to the one in Table 6 of [He et al. \(2016\)](#).

For all the algorithms that we tested, we use the weight decay technique to help improve generalization, which has shown to be effective for both 1st-order ([Loshchilov & Hutter, 2019](#)) and 2nd-order methods ([Zhang et al., 2019](#)). To be more specific, take K-BFGS/K-BFGS(L) (Algorithm 2) as an example, we replace Line 10 with $W_l = W_l - \alpha_k(p_l + \gamma W_l)$ where γ is the weigh decay factor. The same modification is done for SGD-m, Adam, and KFAC as well.

In order to obtain the results in Table 4, we first conducted a grid search for each algorithm based on the following ranges:

- K-BFGS and K-BFGS(L):
 - initial learning rate: { 0.03, 0.1, 0.3, 1, 3, 10, 30, 100, 300, 1e3, 3e3 }
 - weight decay γ : { 1e-7, 1e-6, 1e-5, 1e-4, 1e-3, 0.01, 0.1 }
 - damping (i.e., λ in Algorithm 2): { 1, 10, 100, 1e3, 1e4, 1e5 }
- KFAC:
 - initial learning rate: { 1e-3, 3e-3, 0.01, 0.03, 0.1, 0.3 }
 - weight decay γ : { 0.001, 0.01, 0.1, 1 }
 - damping (i.e., λ in Algorithm 5): { 1e-4, 0.001, 0.01, 0.1, 1, 10, 100 }
- Adam:
 - initial learning rate: { 3e-5, 1e-4, 3e-4, 1e-3, 3e-3, 0.01, 0.03, 0.1 }
 - weight decay γ : { 0.01, 0.1, 1, 10 }
 - damping (i.e., the ϵ HP in [Kingma & Ba \(2014\)](#)): { 1e-8, 1e-4, 0.01, 0.1, 1 }
- SGD-m:
 - initial learning rate: { 3e-4, 1e-3, 3e-3, 0.01, 0.03, 0.1, 0.3 }
 - weight decay γ : { 1e-3, 0.01, 0.1, 1 }

We selected the HP values that achieves the largest classification accuracy on the validation set (see Table 8). We then ran each algorithm with their corresponding best HP values and 5 different random seeds, and reported the average validation classification accuracy in Table 4. The training cross entropy loss (upper rows) and validation classification error (lower

Table 8. Best HP values (initial learning rate, weight decay, damping) for Table 4 as well as Figures 1, 5, 6, and 7

	K-BFGS	K-BFGS(L)	KFAC	Adam	SGD-m
VGG16, CIFAR10	(30, 1e-5, 1e4)	(1, 1e-3, 100)	(0.01, 0.1, 10)	(0.003, 0.1, 0.1)	(0.003, 0.1, -)
ResNet32, CIFAR10	(100, 1e-5, 1e3)	(1e3, 1e-6, 1e4)	(0.01, 0.1, 0.01)	(0.003, 0.1, 0.01)	(0.03, 0.01, -)
VGG16, CIFAR100	(0.1, 0.01, 10)	(0.3, 0.001, 100)	(0.01, 0.1, 1)	(3e-4, 1, 0.01)	(0.003, 0.1, -)
ResNet32, CIFAR100	(1e3, 1e-6, 1e4)	(10, 1e-4, 100)	(0.01, 0.1, 0.001)	(0.01, 0.1, 0.01)	(0.03, 0.01, -)

rows) against number of epochs (left columns) and process time (right columns) are also included in Figure 1 (in Section 6), and Figure 5, 6, and 7 (below).

From Table 8, we can see that, the optimal damping value for K-BFGS and K-BFGS(L) tends to be larger than that for KFAC, which is somewhat reasonable since they use quasi-Newton approaches to estimate curvature information. Hence, a stronger damping term (regularization) is needed. Moreover, in our experiments, for K-BFGS and K-BFGS(L), there was a strong positive correlation between the optimal learning rate and damping values, and a strong negative correlation between the optimal learning rate and weight decay values. These are not surprising because the "effective" learning rate involves the ratio of the learning rate to the damping, and the "effective" weight decay factor is the product of the weight decay value and the learning rate.

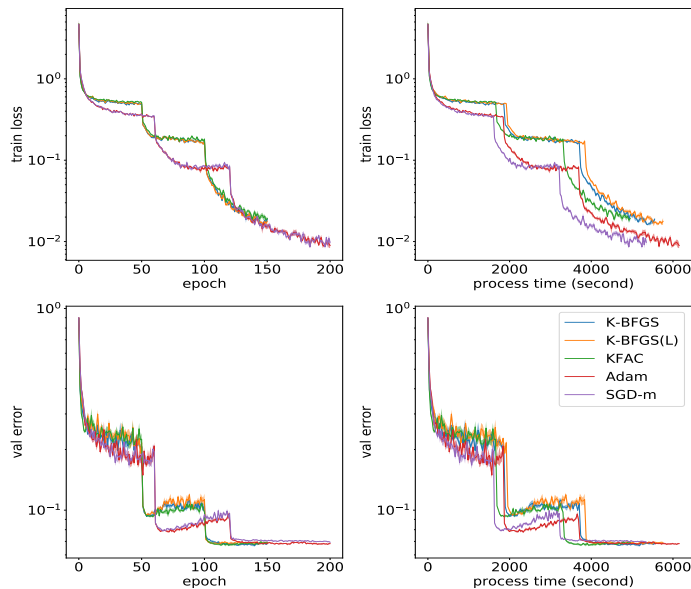


Figure 5. Performance of K-BFGS, K-BFGS(L), KFAC, Adam, and SGD-m on ResNet32 with CIFAR10

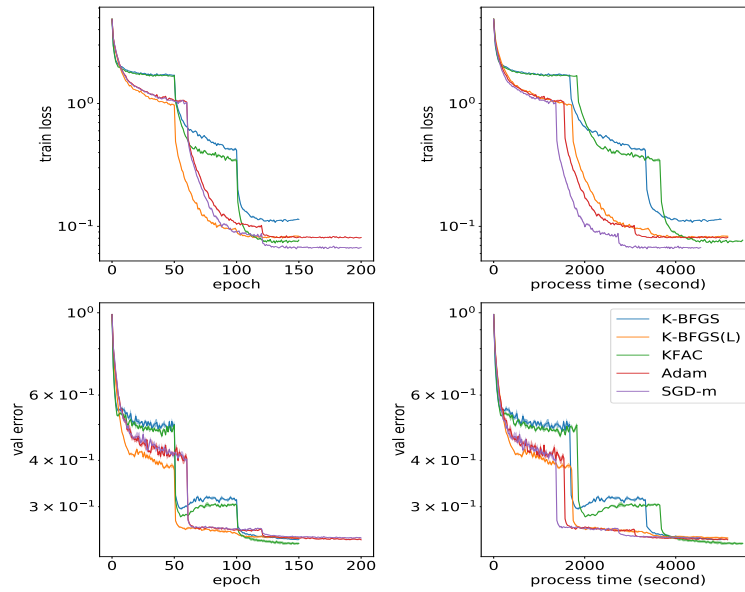


Figure 6. Performance of K-BFGS, K-BFGS(L), KFAC, Adam, and SGD-m on VGG16 with CIFAR100

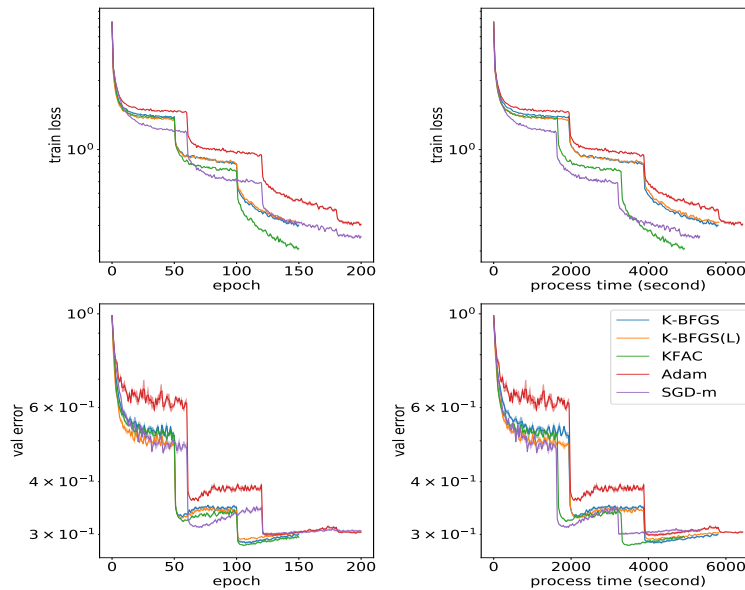


Figure 7. Performance of K-BFGS, K-BFGS(L), KFAC, Adam, and SGD-m on ResNet32 with CIFAR100